ISSN 1068-3739, Russian Meteorology and Hydrology, 2016, Vol. 41, No. 6, pp. 425–434. Allerton Press, Inc., 2016.
Original Russian Text P.S. Verezemskaya, V.M. Stepanenko, 2016, published in Meteorologiya i Gidrologiya, 2016, No. 6, pp. 69–81.

THE WINNERS OF THE CONFERENCE OF YOUNG SCIENTISTS

Numerical Simulation of the Structure and Evolution of a Polar Mesocyclone over the Kara Sea. Part 1. Model Validation and Estimation of Instability Mechanisms

P. S. Verezemskaya[a, b] and V. M. Stepanenko[a]

[a]*Lomonosov Moscow State University, GSP-1, Leninskie Gory, Moscow, 119991 Russia, e-mail: verezemskaya.ps@srcc.msu.ru*

[b]*Shirshov Institute of Oceanology, Russian Academy of Sciences, Nakhimovskii pr. 36, Moscow, 117997 Russia*

Received October 27, 2015

Abstract—Numerical experiments based on the WRF model were conducted to analyze the structure and evolution of the polar mesoscale cyclone developed over the Kara Sea on September 29–30, 2008. It was found that baroclinic instability in the lower troposphere and convective instability (including that due to the wind-induced surface heat exchange) did not play a significant role. Significant contribution was made by the downward advection of potential vorticity from the upper troposphere and by the conditional instability of second kind. It is demonstrated that if water phase transitions are not taken into account, the mesocyclone intensity is reduced by 7–20% and the time of its development increases by 4 hours. The advection of potential vorticity was not the only process causing the intensification of the lower potential vorticity anomaly associated with cyclonic circulation.

DOI: 10.3103/S1068373916060078

Keywords: Polar low, the Arctic, WRF-ARW model, satellite remote sensing

1. INTRODUCTION

Polar lows are intensive mesoscale vortices formed over the open sea surface northward (in the Northern Hemisphere) of the Arctic front in winter and characterized by high wind speed and heavy precipitation [27]. In the Arctic they are dangerous for navigation, oil and gas production, and other economic sectors of the region. The unsatisfactory quality of prediction of lows is caused by their small size and high rate of development and dissipation as well as by the wide range of their types. Under conditions of the current climate change in the Arctic, the area and time period favorable for the formation of lows broaden and the new combinations of factors may become crucial.

According to the point of view that has been generally accepted by the beginning of the 21st century, the development of polar lows cannot be explained with only one physical mechanism. At the initial stages of this process study, baroclinic instability in the lower troposphere on secondary fronts and at the land–sea and ice–sea interfaces [12, 21] as well as the convective instability of cold air flowing to the surface of the relatively warm sea [6, 23] were considered as basic mechanisms. The search of analogies between the formation mechanisms of tropical and polar cyclones [3, 26] resulted in the theory of formation of polar lows due to the mechanism of conditional instability of second kind (CISK) [7] and wind-induced surface heat exchange (WISHE) [11]. As the number of studies based on the results of numerical simulation of mesocyclones was increasing, the interest grew to the investigation of the potential vorticity field and its interaction with baroclinic or conditionally unstable atmosphere [5, 23, 30]. The great progress was made by studying synoptic-scale objects and processes [4, 15]. Based on the theory proposed by B. Hoskins in 1985 [15] and by other authors [10, 24, 25], the classification of extratropical cyclones was developed. It accounts the value of contribution of the advection of vorticity and temperature at upper and lower levels to the development of cyclones as well as the value of the released latent heat of condensation. To attribute the

cyclone to the particular class, the method was used for solution of height-attributable quasi-geostrophic omega equation taking into account vertical motions $_{QG}$ [8, 14].

At present the studies of separate cases of the development of polar lows are based on the joint use of the data of modeling and observations that enables verifying the model and selecting its optimum configuration. The most optimum (from the point of view of spatial and temporal resolution) empirical data for the Arctic are data of satellite multisensor observations. They contain information on two-dimensional horizontal fields and vertical profiles of atmospheric parameters with the measurement frequency of more than twice a day and with the spatial resolution from 75 m to 15 km. Typically, satellite fields are the only available information on real atmospheric conditions in the areas of polar lows emergence.

The mesoscale cyclone formed over the Kara Sea in autumn was chosen for the study. This was caused by the objective of the present paper: to study the mechanisms of generation and intensification of the mesoscale cyclone and their changes in the process of cyclone evolution. We aimed at determining the effects of different factors (baroclinic and convective instability, wind-induced surface heat exchange, water phase transitions, and interlevel potential vorticity exchange) on the polar low dynamics.

2. DATA AND INSTRUMENTS

The identification of the low and its parameters was based on the visible and infrared images of cloudiness and underlying surface obtained from the MODIS spectral radiometer from Terra and Aqua satellites and from the AVHRR radiometer from NOAA satellites. Composite images in RGB format obtained by the combination of MODIS channels 1, 3, and 4 (spatial resolution at nadir is 500 m) and infrared images of channel 31 (resolution is 1 km) were used (http://ladsweb.nascom.nasa.gov/browse_images/). Besides, images from AVHRR channel 5 (spatial resolution at nadir is 1.1 km) were used. As Terra, Aqua, and NOAA satellites operate at sun-synchronous orbits, they provided almost the simultaneous imagery of the same region. The data of AVHRR radiometer were received from NOAA-15, NOAA-16, NOAA-17, and NOAA-18 satellites.

Quantitative characteristics of atmospheric and oceanic parameters were estimated from the data obtained by the advanced microwave scanning radiometer AMSR-E installed at Aqua satellite. The measurement data were taken from the archive of Il'ichev Pacific Oceanological Institute of the Far Eastern Branch of Russian Academy of Sciences (POI FEB RUS) and were borrowed from the Japan Aerospace Exploration Agency Earth Observation Research Center (JAXA/EORC).

Integrated water vapor V (total content (kg/m^2) of water vapor in the vertical atmospheric column of the unit cross-section), cloud liquid water content Q (total content (kg/m^2) of liquid water in the vertical column of the cloud from the base to the top), and surface wind speed U (m/s) characterizing the mesocyclone intensity were estimated using the measured values of brightness temperature $T_{b(\nu)}$ based on the regional polar algorithms which were worked out at POI FEB RUS and Russian State Hydrometeorological University (RSHMU) [33]. The structure of the near-ice-edge zone and the edge position were determined from sea ice concentration maps taken from the website of the University of Bremen (http://www.iup. uni-bremen.de/seaice/amsr/). The fine structure of the surface wind field was investigated using the images received from the Envisat Advanced Synthetic Aperture Radar (ASAR) in the wide swath mode. The data of contact observations were presented in the form of surface and upper-air (850 and 500 hPa) charts for 00:00 UTC on September 30 and October 1, 2008 (archive of the Hydrometcenter of Russia). The fields of potential vorticity were constructed using the ERA-Interim reanalysis data with the resolution of 0.5 0.5 .

3. MESOCYCLONE IN THE KARA SEA

The mesoscale vortex with the diameter of 400 km was detected on two consecutive images received by ASAR from the Envisat satellite at 05:49 and 15:49 UTC on September 30, 2008. The images indicate two stages of the cyclone development. On the surface chart the cyclone was not observed in the form of the system of closed isobars because it was situated in the small trough in the frontal part of the synoptic-scale cyclone whose center was located over the Barents Sea northward of the Kola Peninsula (Fig. 1a). According to data on surface temperature, surface wind, and surface pressure, the cyclone was formed under the influence of southern and southeastern air flows with mean temperature at the height of 2 m 0–2 C. No pronounced atmospheric fronts were observed. Sea surface temperature was 0.1–0.2 C.

The cyclone started being formed at about 05:00 UTC when its cloud system became distinguishable in the AVHRR IR image. It was a spiral of low- and middle-level clouds with two narrow cloud bands of high

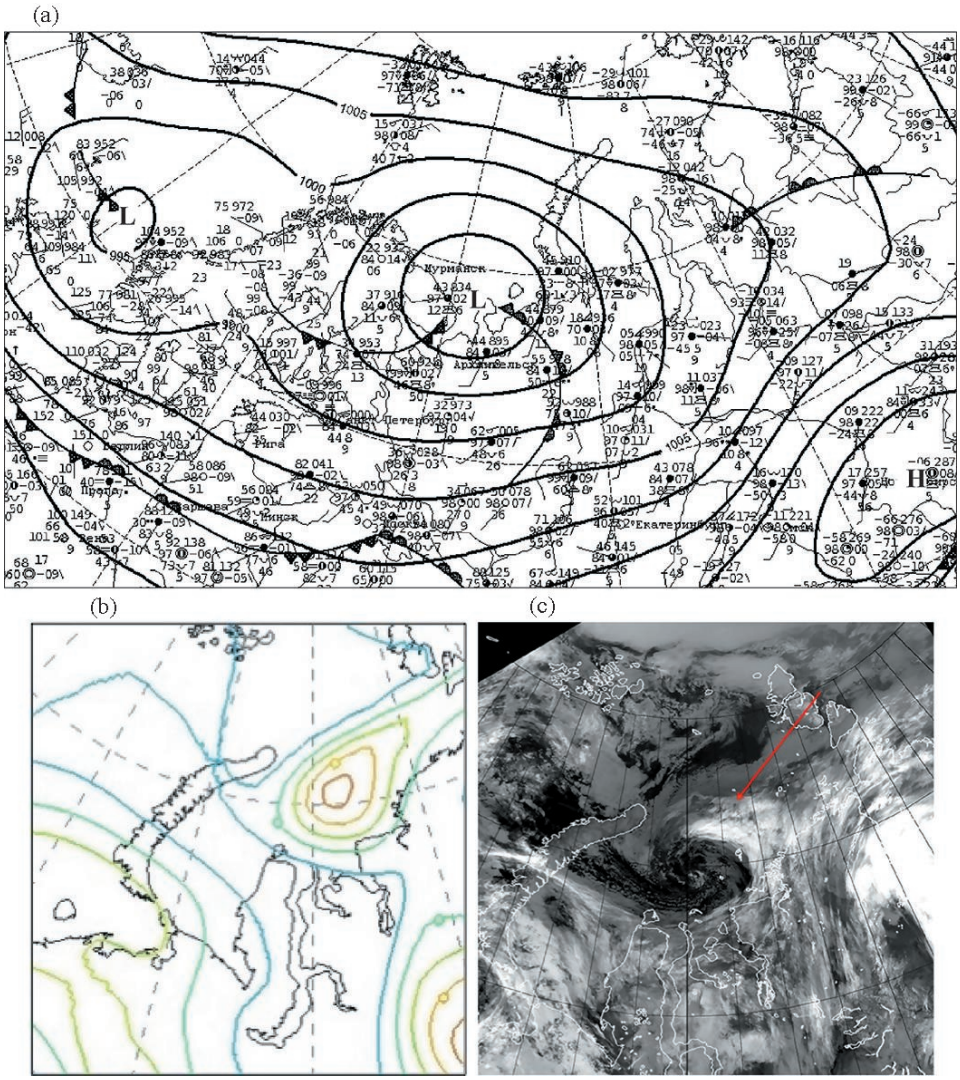

Fig. 1. (a) The surface weather chart (the archive data of the Hydrometcenter of Russia) and (b) potential vorticity field at 00:00 UTC on September 30, 2008; (c) AVHRR IR image of cloudiness on the same day at 14:33 UTC. The maximum value of potential vorticity in the anomaly center in Fig. 1b was equal to 5 PVU. The red arrow in Fig. 1c is the position of the low.

(relative to the neighboring ones) brightness in its center. At the height of 7 km (the level of 300–350 hPa), the positive anomaly of Ertel potential vorticity was present over the area of cyclone generation. The anomaly was detected in the reanalysis field and was supposedly formed on September 28, 2008 after the occlusion of the large-scale cyclone over the Gulf of Ob (Fig. 1b).

The fields of wind speed and cloudiness are in a good agreement not only with each other but also with the fields of atmospheric integrated water vapor and cloud liquid water content. According to the AMSR-E data, at 07:10 UTC the zone with high (relative to the background) values of $V = 10–14$ kg/m^2 corresponded to the cloud spiral, and the zone with $V = 10–12$ kg/m^2 occupied by shallow convection cells, was also observed in the northern part of the cyclone. The bands of convective clouds were represented in the field of liquid water content Q by the zones with the values of 0.1–0.2 kg/m^2. The maximum values of Q were observed closer to the cyclone center where precipitation was likely to take place. The zone of the maximum speed of surface wind $U = 12–14$ m/s was situated in the middle part of the northern spiral.

After that according to cloudiness and wind field, the cyclone intensified (Fig. 2). According to the IR image and microwave radiometer data received at 11:13 UTC (not presented), the vortex moved to the southwest, took the more spiral shape, and the number of convective cloud banks in it increased. By 14:00 UTC the

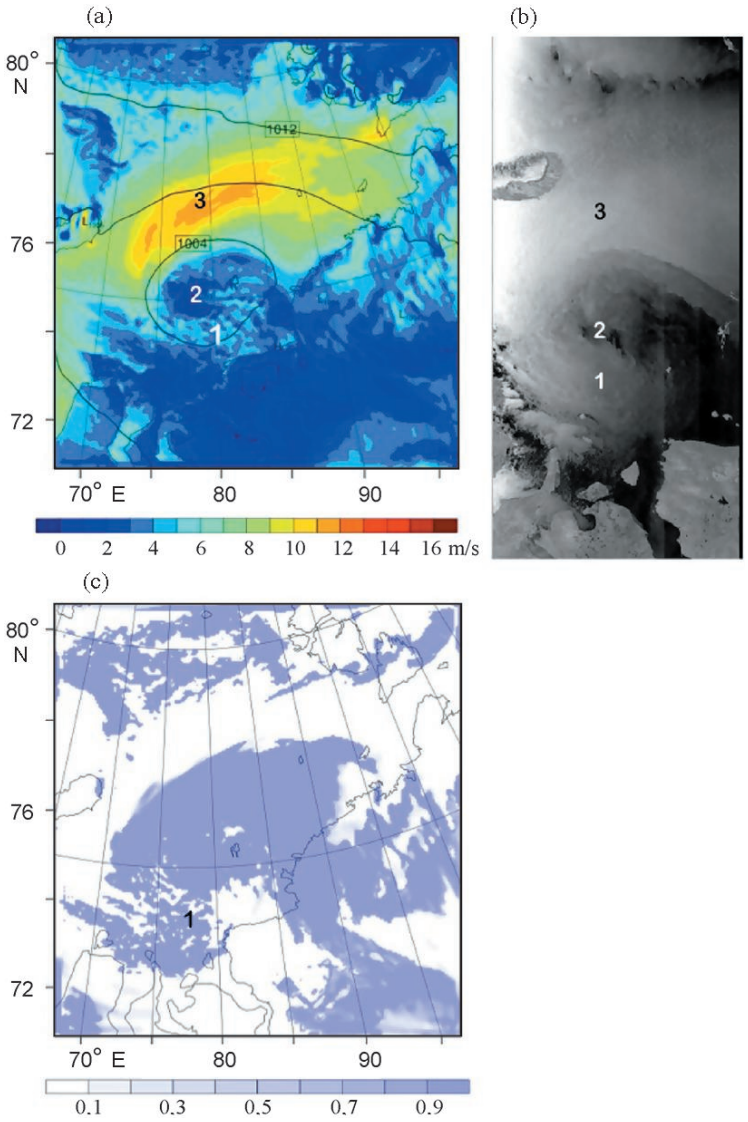

Fig. 2. The fields of (a) wind speed at the height of 10 m and (c) the amount of cloudiness (in unit fractions) at the height of 1300 m from the data of the WRF base experiment at 16:00 UTC and (b) the ASAR image received at 15:49 UTC on September 30, 2008. (1) Convective cells; (2) the calm zone; (3) the zone of maximum wind.

maximum wind speed reached 15 m/s. It is obvious from the ASAR image that wind shear lines corresponded to these convective bands at 15:49 UTC. The cloudless and low-wind zone with the diameter of about 30–50 km was situated in the vortex center. By 22:05 UTC the cloud system area decreased but continued swirling. As compared with the previous time moment, integrated water vapor content increased and was equal to 13–14 kg/m^2. Liquid water content decreased because water turned into crystals. Wind speed decreased to 13–14 m/s at 22:05 UTC and was equal to 10–12 m/s at 23:49 UTC. The stage of the maximum development of the cyclone had been passed by that moment.

4. NUMERICAL EXPERIMENTS WITH WRF-ARW MODEL

Numerical experiments were based on the WRF-ARW three-dimensional nonhydrostatic model [17–20, 28, 29].

To determine a role of water phase transitions, two numerical experiments were conducted: with the enabled (the base experiment) and disabled scheme of phase transitions in the atmosphere. The numerical experiments were conducted on the Lomonosov supercomputer [31]. The run time for each of them was

5 hours of computer time at 64 computing cores. The data of ERA-Interim reanalysis of European Centre for Medium-range Weather Forecasts at standard levels with the spatial resolution of 0.25 0.25 and with the temporal resolution of 6 hours were used as initial and boundary conditions. The time and dates of the start and end of model integration were the same in both experiments, that is, from 12:00 UTC on September 29 to 12:00 UTC on October 1, 2008. The integration domain covered the Kara Sea area from 70 to 81 N and from 65 to 100 E. The model grid transformations associated with transition to rectangular coordinates were carried out according to polar stereographic projection. The horizontal grid spacing was equal to 5 km. Fifty levels of -coordinate were specified in the vertical direction. The upper boundary of the domain was located at the level of 50 hPa. All parameters in the block of physical parameterizations (except the microphysics scheme) were common for two experiments. To select parameterization schemes for subgrid processes, the results of Atmospheric Model Parameterizations in the Polar Regions Workshop held in 2012 (Boulder, Colorado, USA) and the data presented in [1] were taken into account.

The processes of the transport of long- and short-wave radiation were described in accordance with the CAM (Community Atmospheric Model) parameterization [9]. The processes in the surface layer were described using the scheme based on the Monin–Obukhov similarity theory [34] supplemented with the description of the laminar sublayer. The Noah scheme was chosen to simulate processes on the land surface and in the active layer [32]. The vertical eddy transport and the calculation of the profiles of lows in the atmospheric boundary layer were based on the Mellor–Yamada–Janjic scheme where the equation of turbulent kinetic energy with the constants proposed in [16] is used to compute the vertical diffusion coefficient. The "Rayleigh sponge" was used in order to absorb gravity waves at the upper boundary of the domain. Microphysical processes in the base experiment were accounted for the Goddard single-moment scheme based on the Lin scheme [21].

5. DIAGNOSIS OF HYDRODYNAMIC INSTABILITY MECHANISMS

To analyze the process of formation and evolution of the above mesocyclone, the parameters were computed which characterize the intensity of different mechanisms of polar low development. These mechanisms include baroclinic instability, convective instability, conditional instability of second kind (CISK), wind-induced surface heat exchange (WISHE), and interaction between potential vorticity anomalies at different levels.

Baroclinic instability. In the absence of surface perturbation in the pressure field the polar low may start developing against a background of interaction between the upper-level trough and the surface baroclinic zone [24]. The circulation associated with the upper trough may be a reason for the initial perturbation in the field of isotherms in the lower troposphere if the static stability of the atmosphere is low and the size of upper anomaly is large [22]. This is possible if the Rossby vertical propagation scale [13] is equal to or is more than the physical distance between the upper-level trough and the surface baroclinic zone:

$$H \quad \frac{fL}{N} \tag{1}$$

where N is the mean Brunt–Väisälä frequency in the layer under consideration; f is the Coriolis parameter; L is the phenomenon horizontal scale. By the computation of this parameter we assessed the possibility of interaction of two anomalies of potential vorticity, namely, the lower (the level of 850 hPa) anomaly related to the polar low circulation and the upper (the level of 400 hPa) anomaly.

The potential of baroclinic mechanism for the vortex-scale wave to lose its stability, was assessed with the stability criterion used in the Eady problem [2]:

$$\frac{NkH}{f_0} \tag{2}$$

where H is the vertical extent of the baroclinic zone; $k = 2 /L$ is the wave number, L is the wavelength (the zone horizontal extent); f_0 is the Coriolis parameter at the latitude of 45 (it is used because the Eady problem does not take into account the beta effect). At the fixed static stability of the atmosphere the waves are stable if $> _{cr} = 2.399$.

Convective instability. In the class of convective instability, CISK and WISHE mechanisms are of special importance for cyclogenesis. With regard to polar lows both mechanisms are the cycles of positive feedback where vorticity increases due to convection-induced heating in the middle troposphere. The main difference consists in the conditions and mechanisms of convection triggering: CISK assumes the conditionally unstable atmosphere with stored instability energy [26] whereas WISHE initiates heating using

turbulent fluxes of latent and sensible heat at the surface in the atmosphere whose conditions are close to neutral [12]. It should be noted that neither CISK nor WISHE explain causes for the formation of initial perturbation and require the already existing cyclonic vortex to start the intensification mechanism.

6. RESULTS

Comparison with observational data. The WRF model simulates the general structure of the vortex successfully: the bands of convective clouds observed in the ASAR image in the southern part of the cyclone are well distinguished in the simulated fields of wind speed and cloudiness (Fig. 2). The location of the zones of maximum wind speed and low-wind in the cyclone central part also corresponds to the observational data.

The distribution of wind speed of >10 m/s in the model field follows the configuration observed in the radiometer field, and its values are equal to 12 m/s (Fig. 2). In the field of integrated water vapor V the model simulates the zone of higher (as compared to the neighboring ones) values (7.2 kg/m^2); however, in the northeastern part of the spiral the value of integrated water vapor is by 1.5–2 kg/m^2 smaller than that obtained from observations (13 kg/m^2). This is also observed for the previous time moment. The vortex structure is significantly disturbed in the simulated fields of the experiment with the disabled parameterization of microphysics; however, the decrease in integrated water vapor in the cyclone does not take place because water vapor sink is absent as a result of condensation and sublimation.

Structure and evolution of mesocyclone. The base experiment. Let us consider the main characteristics of the mesocyclone obtained from the modeling data. The mesocyclone was generated in the field of surface pressure in the form of the closed isobar at 12:00 UTC on September 30, 2008 after the trough where it was generated, started being observed on the water surface. During the next 20 hours the cyclone was developing and intensifying, the diameter of the area of the outer closed isobar was increasing, and the precipitation associated with clouds in the northeastern part of the spiral was increasing as well. The minimum pressure in the cyclone was equal to 1002.7 hPa and was reached by about 20:00 UTC according to the model data. Neither the considerable horizontal temperature gradient (the gradient in the layer from 0 to 4 km was equal to 1–4.5 C/100 km) nor conditions for cold intrusion were observed in the zone of cyclone generation because temperature in the lower troposphere was almost equal to that inside the vortex (1–2 C). The weak baroclinic zone (with the temperature gradient of 5–7 C/100 km) was detected in the layer of 3–4 km. The reason for its formation was the bend of isentropes associated with the anomaly of potential vorticity at the height of 7 km. With time temperature in the cold center of the cyclone in the middle troposphere rose from –21 to –19 C. The estimate of stability criterion in the layer of 1–4 km for the zone of high (relative to background values) temperature gradient (~500 km) demonstrated that the wave with such length is stable under the observed conditions: = 3.975 > $_{cr}$ (Fig. 3).

The atmosphere was stratified stably, the increase in potential temperature with height was observed in the whole integration domain, and the Brunt–Väisälä frequency varied from 0.012 to 0.015 s^{-1} for the whole period of modeling. It should be noted that CAPE (convective available potential energy) was absent from the atmosphere both at the initial and next time moments. The values of fluxes of sensible and latent heat from the sea surface during the cyclone lifetime were small due to insignificant difference between the temperature of air and water and due to the stable stratification of the atmosphere in the surface layer. At the stage of its maximum development the value of these fluxes was equal to 64 and 82 W/m^2, respectively.

The anomaly of potential vorticity (PV) at the level of 300 hPa with the maximum value in its central part reaching 9 PVU (1 PVU = 10^{-6} K m^2 kg^{-1} s^{-1}) was situated westward of the low and preceded its generation. In the process of the vortex intensification the anomaly was moving to the northeast and was weakening. The interaction between the upper anomaly and the lower anomaly related to the convergence in the surface layer could have taken place because the Rossby propagation scale was 6800 m and exceeded the physical distance (5120 m) between the anomalies at the levels of 400 and 850 hPa. The advective transport was not the crucial mechanism of vorticity transfer from the upper anomaly to the lower one because, according to the computations, it was equal to 2 10^{-5} PVU/s whereas the trend in the lower anomaly of the potential vorticity was equal to 6 10^{-5} PVU/s. With time the lower anomaly of potential vorticity increased and was equal to 1.5–3 PVU at the level below 850 hPa at the moment of its maximum development. At that time the lower anomaly was situated directly over the upper one; therefore, the zones coincided of upward and downward motions associated with the anomalies. Since 02:00 UTC on October 1, 2008 the surface anomaly moved to the west of the upper one. As a result, the vertical motions associated with it were suppressed by those related to the upper anomaly. After that the anomaly continued moving to the west and caused the subsequent destruction of the low.

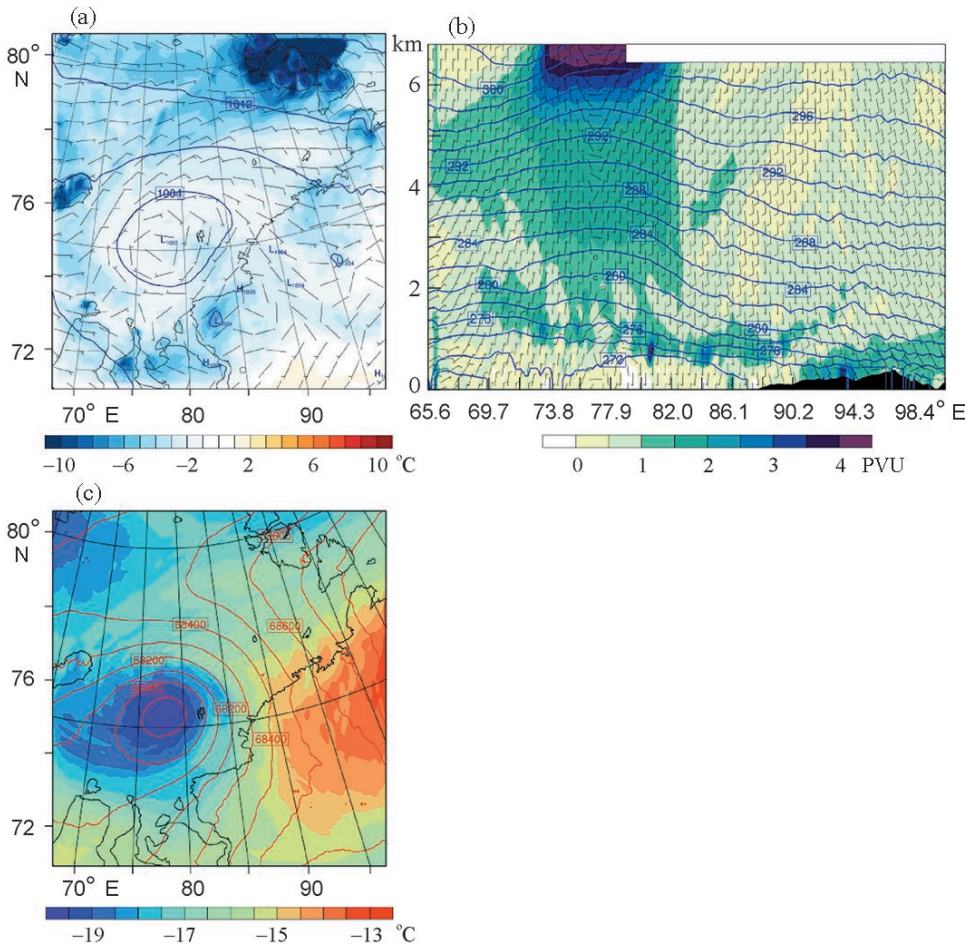

Fig. 3. (a) The field of sea-level pressure, temperature, and wind speed near the surface, (b) the vertical cross-section of the field of Ertel potential vorticity through the center of the low, and (c) the field of air temperature and geopotential at the height of 3 km at 18:00 UTC on September 30, 2008.

By 14:00 UTC on October 1, 2008 the closed isobar of 1004 hPa disappeared in the pressure field over the sea surface.

Phase transition effect. The comparison between the results of the experiment with disabled phase transitions and the fields of parameters obtained in the base experiment revealed that in the mesocyclone intensification a significant role is played by latent heat release in the process of condensation in the middle troposphere due to the CISK mechanism. The intensity of the low decreases in the absence of water phase transitions. As the factor of increase in vorticity due to the heating in the middle troposphere is also observed at the trough stage (till 12:00 UTC), the cyclone is formed in the field of pressure 4 hours later than the real time of its formation registered from satellite data. The intensity of the lower anomaly does not exceed 1 PVU over the whole lifetime of the low; the values of more than 2 PVU related to the upper anomaly are observed to the height of 3 km only (Fig. 4).

The maximum wind speed decreases by 2 m/s on average and the minimum pressure in the cyclone is 1003 hPa; however, the configuration and time needed to reach different stages of the vortex maturity vary between two experiments. The maximum value of the fluxes of sensible and latent heat from the surface does not exceed 30 and 40 W/m^2, respectively.

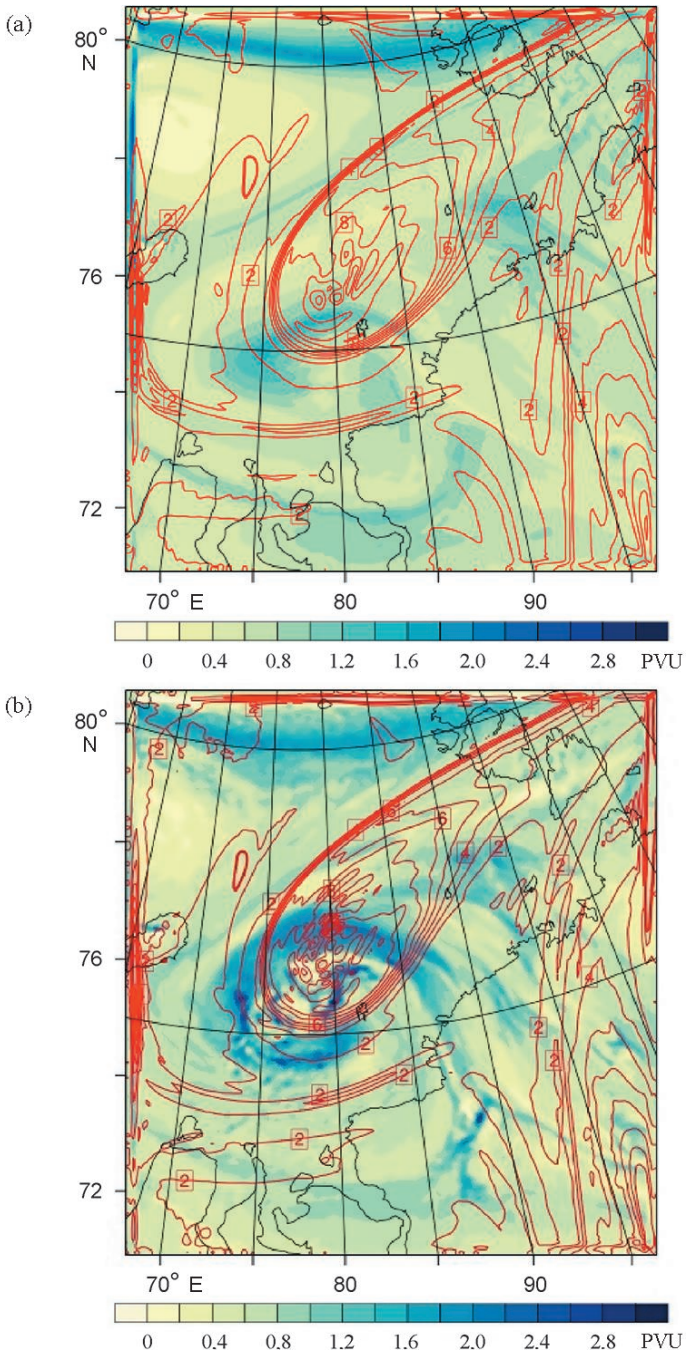

Fig. 4. The anomalies of potential vorticity at the level of 850 hPa (color) and 400 hPa (the isolines) at 18:00 UTC on September 30, 2008 from the data of the experiment with (a) the disabled and (b) enabled parameterization of microphysical processes.

7. CONCLUSIONS

Using the data of satellite observations and numerical simulation, the structure and evolution of the mesoscale cyclone generated on September 30, 2008 over the Kara Sea are considered. Its formation was not caused by "classic" preconditions; the atmosphere was stratified stably and no considerable horizontal temperature gradient and significant heat fluxes from the sea surface were observed. Hence, this low was generated not only as a result of the interaction between the upper- and lower-level anomalies of potential vorticity but also under the influence of condensation latent heat release in the middle troposphere. The dis-

able of CISK representation in the model reduces the cyclone intensity by 7–20% basically due to the absence of moisture convergence increase in the lower troposphere without the source of heat at middle levels. The interaction between the anomalies of potential vorticity under the observed conditions was possible; however, it was realized not only through advection. The next paper will study the mechanisms of potential vorticity transfer between anomalies at different levels in this cyclone.

ACKNOWLEDGMENTS

The research was supported by the Russian Foundation for Basic Research (grant 14-05-00959).

REFERENCES

1. P. S. Verezemskaya and V. M. Stepanenko, "Numerical Simulation of Intense Polar Mesoscale Cyclones with the WRF Model," in *International Conference and School of Young Scientists on Measurements, Modeling, and Information Systems for Environmental Studies* (Tomskii TsNTI, Tomsk, 2014) [in Russian].
2. E. M. Volodin and V. N. Lykosov, "Parameterization of Heat and Moisture Transfer in the Soil–Vegetation System for Use in Atmospheric General Circulation Models: 1. Formulation and Simulations Based on Local Observational Data," Izv. Akad. Nauk, Fiz. Atmos. Okeana, No. 4, **34** (1998) [Izv., Atmos. Oceanic Phys., No. 4, **34** (1998)].
3. G. S. Golitsyn, "Polar Lows and Tropical Hurricanes: Their Energy and Sizes and a Quantitative Criterion for Their Generation," Izv. Akad. Nauk, Fiz. Atmos. Okeana, No. 5, **44** (2008) [Izv., Atmos. Oceanic Phys., No. 5, **44** (2008)].
4. F. Ahmadi-Givi, G. C. Craig, and R. S. Plant, "The Dynamics of a Midlatitude Cyclone with Very Strong Latent Heat Release," Quart. J. Roy. Meteorol. Soc., No. 596, **130** (2004).
5. T. J. Bracegirdle and S. L. Gray, "The Dynamics of a Polar Low Assessed Using Potential Vorticity Inversion," Quart. J. Roy. Meteorol. Soc., No. 641, **135** (2009).
6. S. Businger, "The Synoptic Climatology of Polar Low Outbreaks," Tellus A, No. 5, **37** (1985).
7. J. G. Charney and A. Eliassen, "On the Growth of the Hurricane Depression," J. Atmos. Sci., No. 1, **21** (1964).
8. S. A. Clough, C. S. A. Davitt, and A. J. Thorpe, "Attribution Concepts Applied to the Omega Equation," Quart. J. Roy. Meteorol. Soc., No. 536, **122** (1996).
9. W. D. Collins, P. J. Racsh, B. A. Boville, et al., *Description of the NCAR Community Atmosphere Model (CAM 3.0)*, Tech. Rep. NCAR/TN-464+ STR (2004).
10. A. C. L. Deveson, K. A. Browning, and T. D. Hewson, "A Classification of FASTEX Cyclones Using a Height-attributable Quasi-geostrophic Vertical Motion Diagnostic," Quart. J. Roy. Meteorol. Soc., No. 579, **128** (2002).
11. K. A. Emanuel and R. Rotunno, "Polar Lows as Arctic Hurricanes," Tellus A, No. 1, **41** (1989).
12. I. Fore, J. E. Kristjansson, E. W. Kolstad, et al., "A Hurricane-like Polar Low Fuelled by Sensible Heat Flux: High Resolution Numerical Simulations," Quart. J. Roy. Meteorol. Soc., No. 666, **138** (2012).
13. J. R. Holton and G. J. Hakim, *An Introduction to Dynamic Meteorology* (Academic Press, 2013).
14. B. J. Hoskins, I. Draghici, and H. C. Davies, "A New Look at the Omega-equation," Quart. J. Roy. Meteorol. Soc., No. 439, **104** (1978).
15. B. J. Hoskins, M. E. McIntyre, and A. W. Robertson, "On the Use and Significance of Isentropic Potential Vorticity," Quart. J. Roy. Meteorol. Soc., No. 470, **111** (1985).
16. Z. I. Janjic, "Nonsingular Implementation of the Mellor–Yamada Level 2.5 Scheme in the NCEP Meso Model," NCEP Office Note, **437** (2002).
17. A. Kasahara, "Various Vertical Coordinate Systems Used for Numerical Weather Prediction," Mon. Wea. Rev., No. 7, **102** (1974).
18. J. B. Klemp, W. C. Skamarock, and J. Dudhia, "Conservative Split-explicit Time Integration Methods for the Compressible Nonhydrostatic Equations," Mon. Wea. Rev., **135** (2007).
19. J. B. Klemp and R. B. Wilhelmson, "The Simulation of Three-dimensional Convective Storm Dynamics," J. Atmos. Sci., No. 6, **35** (1978).
20. R. Laprise, "The Euler Equations of Motion with Hydrostatic Pressure as an Independent Variable," Mon. Wea. Rev., No. 1, **120** (1992).
21. Y.-L. Lin, R. D. Farley, and H. D. Orville, "Bulk Parameterization of the Snow Field in a Cloud Model," J. Climate and Appl. Meteorol., **22** (1983).
22. M. T. Montgomery and B. F. Farrell, "Polar Low Dynamics," J. Atmos. Sci., No. 24, **49** (1992).
23. T. E. Nordeng and E. A. Rasmussen, "A Most Beautiful Polar Low. A Case Study of a Polar Low Development in the Bear Island Region," Tellus A, No. 2, **44** (1992).
24. S. Peterssen and S. J. Smebye, "On the Development of Extratropical Cyclones," Quart. J. Roy. Meteorol. Soc., No. 414, **97** (1971).

25. R. S. Plant, G. C. Craig, and S. L. Gray, "On a Threefold Classification of Extratropical Cyclogenesis," Quart. J. Roy. Meteorol. Soc., No. 594, **129** (2003).
26. E. Rasmussen, "The Polar Low as an Extratropical CISK Disturbance," Quart. J. Roy. Meteorol. Soc., No. 445, **105** (1979).
27. E. A. Rasmussen and J. Turner, *Polar Lows: Mesoscale Weather Systems in the Polar Regions* (Cambridge Univ. Press, 2003).
28. W. C. Skamarock, J. B. Klemp, J. Dudhia, et al., *A Description of the Advanced Research WRF Version 3*, Technical Report (2008).
29. W. C. Skamarock and M. L. Weisman, "The Impact of Positive-definite Moisture Transport on NWP Precipitation Forecasts," Mon. Wea. Rev., No. 1, **137** (2009).
30. M. T. Stoelinga, "A Potential Vorticity-based Study of the Role of Diabatic Heating and Friction in a Numerically Simulated Baroclinic Cyclone," Mon. Wea. Rev., No. 5, **124** (1996).
31. V. V. Voevodin, S. A. Zhumatiy, S. I. Sobolev, et al., "Practice of "Lomonosov" Supercomputer," Open Systems J., **7** (2012).
32. Z.-L. Yang, G.-Y. Nio, K. E. Mitchell, et al., "The Community Noah Land Surface Model with Multiparameterization Options (Noah-MP): 2. Evaluation over Global River Basins," J. Geophys. Res., **116** (2011).
33. E. V. Zabolotskikh, L. M. Mitnik, and B. Chapron, "New Approach for Severe Marine Weather Study Using Satellite Passive Microwave Sensing," Geophys. Res. Lett., No. 13, **40** (2013).
34. S. Zilitinkevich, "Non-local Turbulent Transport Pollution Dispersion Aspects of Coherent Structure of Convective Flows," in *Air Pollution III, Air Pollution Theory and Simulation*, Ed. by H. Power, N. Moussiopoulos, and C. A. Brebbia (Computational Mechanics Publ., Southampton, Boston 1, 1995).